Quaternary Science Reviews 192 (2018) 59–70

Contents lists available at ScienceDirect

Quaternary Science Reviews

journal homepage: www.elsevier.com/locate/quascirev

Holocene paleoceanography of Bigo Bay, west Antarctic Peninsula: Connections between surface water productivity and nutrient utilization and its implication for surface-deep water mass exchange

Sunghan Kim [a], Kyu-Cheul Yoo [a, *], Jae Il Lee [a], Boo-Keun Khim [b], Young-Suk Bak [c], Min Kyung Lee [a], Jongmin Lee [b], Eugene W. Domack [d, 1], Andrew J. Christ [e], Ho Il Yoon [a]

[a] Korea Polar Research Institute, Incheon, 21990, South Korea
[b] Department of Oceanography, Pusan National University, Busan, 46241, South Korea
[c] Department of Earth and Environmental Sciences, Chonbuk National University, Jeonju, 54896, South Korea
[d] College of Marine Science, University of South Florida, Tampa, FL, 33620, USA
[e] Department of Earth & Environment, Boston University, Boston, MA, 02115, USA

ARTICLE INFO

Article history:
Received 27 December 2017
Received in revised form
23 April 2018
Accepted 20 May 2018
Available online 30 May 2018

Keywords:
Holocene
Paleoceanography
West Antarctic Peninsula
Marine core
Geochemistry
Nutrient utilization

ABSTRACT

Paleoceanographic changes in response to Holocene climate variability in Bigo Bay, west Antarctic Peninsula (WAP) were reconstructed through geochemical, isotopic, sedimentological, and microfossil analysis. Core WAP13-GC47 is composed of 4 lithologic units. Unit 4 was deposited under ice shelf settings. Unit 3 represents the mid-Holocene open marine conditions. Unit 2 indicates lateral sediment transport by a glacier advance during the Neoglacial period. The chronological contrast between the timing of open marine conditions at core WAP13-GC47 (*ca.* 7060 cal. yr BP at 540 cm) and the ages of calcareous shell fragments (*ca.* 8500 cal. yr BP) in Unit 2b suggests sediment reworking during the Neoglacial period. Unit 1 was deposited during the Medieval Warm Period (MWP) and the Little Ice Age (LIA). Surface water productivity, represented by biogenic opal and total organic carbon (TOC) concentrations, increased and bulk $\delta^{15}N$ (nitrate utilization) decreased during the warmer early to middle Holocene and the MWP. In contrast, surface water productivity decreased with increased bulk $\delta^{15}N$ during the colder Neoglacial period and LIA in Bigo Bay. The nitrate utilization was enhanced during cold periods in association with strong surface water stratification resulting from increased sea ice meltwater discharge or proximity to an ice shelf calving front in Bigo Bay. Reduced nitrate utilization during warm periods is related to weak stratification induced by less sea ice meltwater input and stronger Circumpolar Deep Water influence.

1. Introduction

The west Antarctic Peninsula (WAP) is among the most rapidly warming areas in the world (e.g., King, 1994; Vaughan et al., 2003; Cook et al., 2016) where atmospheric mean air temperatures rose 2.5 °C in the Antarctic Peninsula from A.D. 1950 to 2000 (Turner et al., 2005). This warming has been accompanied by a general trend of ongoing glacial retreat in the WAP that initiated between A.D. 1955 and 1969 (Cook et al., 2005a, 2016; Rignot et al., 2014). Additionally, winter sea ice duration in the WAP is decreasing in response to recent warming (e.g., Smith and Stammerjohn, 2001; Vaughan et al., 2003; Stammerjohn et al., 2008). Dramatic, rapid increases in the near-surface temperature over the last few decades were observed along the WAP (Cape et al., 2015 and references therein). Accordingly, the transition from a polar to subpolar climate in the WAP has profound impacts upon surface water production, with phytoplankton biomass decreasing in the north and increasing further south since the late A.D. 1970s (Montes-Hugo et al., 2009). Given the host of recent, rapid, and interconnected climatological, biological, oceanographic, and glaciological changes across this region, studies of Holocene paleoceanographic changes associated with the AP ice sheet are paramount to understanding the region's future vulnerability to climate change.

* Corresponding author.
E-mail address: kcyoo@kopri.re.kr (K.-C. Yoo).
[1] Deceased in November, 2017.

https://doi.org/10.1016/j.quascirev.2018.05.028
0277-3791/

Decades of marine sediment core studies of the Antarctic continental shelf revealed a suite of marine sediment facies that correspond to past glacio-marine environments (Domack et al., 2003; Hillenbrand et al., 2010) and reconstruct the spatio-temporal variations of grounded ice in the WAP since the Last Glacial Maximum (LGM) (Larter et al., 2014; The RAISED Consortium et al., 2014). In the Amundsen Sea and Bellingshausen Sea sectors of the WAP, the LGM ice sheet remained in the outer to middle shelf area until 5 ka, but rapidly retreated toward the modern positions in the inner shelf (Larter et al., 2014). Given this apparent sensitivity of grounded ice on the inner shelf, a deglacial history of this region may provide important insights for future climatic change. The proximity of inner shelf sediment records to the grounded ice margin provides greater potential to detect past grounding line fluctuations. Despite dynamic – and often complex – deglaciation patterns of the inner shelf (Allen et al., 2010 and references therein), inner shelf records back to the earliest Holocene from WAP fjords remain to be studied in depth.

Upwelling and intrusion of relatively warm and saline Circumpolar Deep Water (CDW) onto the WAP shelf (Smith et al., 1999; Smith and Klinck, 2002; Klinck et al., 2004; Jenkins and Jacobs, 2008; Moffat et al., 2009) enhances basal melting in the sub-ice shelf cavity that accelerates grounding line retreat and ice shelf collapse (Klinck et al., 2004; Bentley et al., 2005; Rignot, 2006; Smith et al., 2007a). During the Little Ice Age (LIA) reduced upwelling and influence of the CDW onto the WAP shelf may have facilitated local ice shelf expansion (Ishman and Domack, 1994; Domack et al., 1995; Bentley et al., 2005; Christ et al., 2015). Surface water productivity also presumably changed in response to CDW upwelling variability due to its enriched nutrient content. Primary productivity increased under open ocean conditions during the warmer mid-Holocene, whereas primary productivity decreased synchronously with greater sea ice coverage during the colder Neoglacial period (e.g., Domack et al., 1995; Shevenell et al., 1996; Taylor et al., 2001; Brachfeld et al., 2003; Domack et al., 2003; Allen et al., 2010; Christ et al., 2015). Although the variability of the CDW intrusion onto the WAP shelf areas is demonstrably related to environmental changes in the WAP (Domack et al., 2003), the role of the CDW in nutrient utilization across the WAP has not been discussed, despite the water mass's enriched nutrient character (Ainley and Jacobs, 1981; Jacobs et al., 1985; Castagno et al., 2017). The nutrient cycle in the WAP shelf can, therefore, be related to and understood in the context of past changes in surface water productivity and degree of upwelling/stratification.

In this study, we compiled a multi-proxy record from sediment cores collected from outer and inner Bigo Bay, WAP that includes: magnetic susceptibility (MS), water content (WC), biogenic opal concentrations, total organic carbon (TOC), total nitrogen (TN), $CaCO_3$, diatom assemblage analysis, and bulk $\delta^{15}N$, a proxy for nitrate utilization (e.g., Francois et al., 1992; Altabet and Francois, 1994). Here, we reconstruct Holocene deglaciation patterns and paleoceanographic changes, including surface water productivity and nutrient utilization, in the WAP, and improve upon previously poorly reported proxies, such as bulk $\delta^{15}N$, biogenic opal, and $CaCO_3$ concentrations in relation to other sedimentological observations.

2. Study area

Bigo Bay (65°43′S, 64°30′W; Fig. 1) is a small (~15 km long by ~11 km wide), northwest-southeast-trending fjord in the west Graham Land coast along the Grandidier Channel bordered by Leroux Bay to the north and Barilari Bay to the south (Fig. 1). Bigo Bay is characterized by over-deepened basins that range in depth between 520 and 700 m, as well as several shallow areas (>50 m) and small glaciated islands. Comrie Glacier and several small unnamed marine-terminating glaciers drain into Bigo Bay (Fig. 1). Historic records of ice front positions document the decay of a small ice shelf pinned between Lizard Island and the northern wall of the fjord (Ferrigno et al., 2008).

The Antarctic Circumpolar Current (ACC) flows clockwise in a broad zone around Antarctica (Fig. 1). Strong surface circulation of the upper layer (50–100 m depth) near the shelf slope is associated with the eastward flow of the southernmost front of the ACC (Meredith et al., 2010). This flow can form semi-closed gyre-like circulations over the outer shelf and intrude onto the shelf in places, most notably toward the northern end of the WAP (Klinck et al., 2004). Spring and summer melt of sea ice and glacial ice decreases surface water density and forms Antarctic Surface Water (AASW), a water mass that is also important for upper layer circulation in the WAP (Meredith et al., 2010). A pycnocline separates AASW from deeper circulation dominated by the CDW derived from the ACC (Meredith et al., 2010). The CDW, an intermediate depth water mass, is relatively warm (>1.5 °C), salty (34.65–34.7‰), and nutrient rich (Ainley and Jacobs, 1981; Jacobs et al., 1985; Castagno et al., 2017). Although the CDW exists at depths below 200 m, this water mass can upwell onto and flow across the WAP shelf through over-deepened troughs carved by paleo-ice streams that extend from the continental shelf break to the inner shelf (e.g., Klinck, 1998; Smith et al., 1999; Smith and Klinck, 2002; Klinck et al., 2004; Martinson et al., 2008). Intrusions of warm, saline, and nutrient-rich CDW onto the shelf interact with and are modified by, overlying water masses (Hofmann et al., 1996; Klinck, 1998; Smith et al., 1999). The rugged, glacially sculpted bathymetry of the inner WAP shelf may contribute to and enhance water mass mixing (Bentley et al., 2009).

Sea ice may play an important role in environmental changes around the WAP (e.g., Shevenell et al., 1996; Vaughan et al., 2003; Allen et al., 2010). Freshwater input through sea ice melt enhances ocean surface water stratification; therefore, it is important to understand the changes in the freshwater budget of the WAP across a range of time-scales (Meredith et al., 2010). A thin layer of sea ice melt generated during the spring can greatly stabilize the surface ocean to create a favorable light environment that may encourage phytoplankton bloom development by retaining the biological cells (Mitchell and Holm-Hansen, 1991). Glacial meltwater can provide similar conditions (Dierssen et al., 2002), along with a potential supply of micronutrients (such as iron) sourced from glacial scouring of underlying bedrock and sediment to the surface ocean, as well as micro-nutrient accumulation via atmospheric deposition (Meredith et al., 2010).

This multi-proxy record from outer and inner Bigo Bay provides the opportunity to examine Holocene paleoclimate variability and its effect upon the dynamics of marine-terminating glaciers, sea ice, and water masses on the inner shelf of the WAP.

3. Material and methods

Three shallow sediment cores were collected from Bigo Bay by the R/V *Araon* during the ANA03C Cruise in 2013, including: a 5.63 m long gravity core WAP13-GC47 (65°36.7675′S, 64°45.5070′W, 673 m water depth) and a 0.42 m long box core WAP13-BC47 (65°36.7675′S, 64°45.5070′W, 673 m water depth) from the outer fjord, and a 6.79 m long gravity core WAP13-GC45 (65°45.1004′S, 64°31.4884′W, 516 m water depth) from the inner fjord (Fig. 1b).

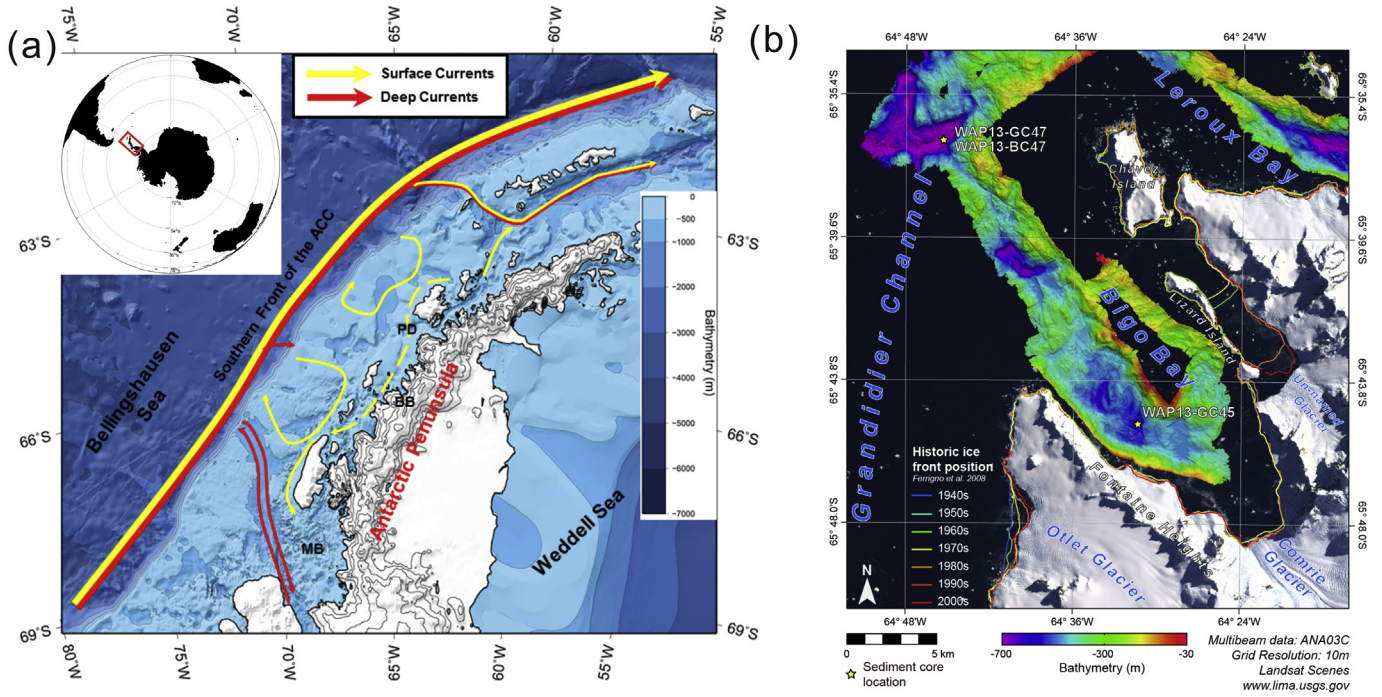

Fig. 1. (a) Regional overview map of the Antarctic Peninsula with schematic ocean circulation. Yellow arrows show surface circulation patterns and red arrows show deep circulation (i.e., Circumpolar Deep Current). This figure is modified from Meredith et al. (2010) and Bentley et al. (2005). ACC: Antarctic Circumpolar Current, PD: Palmer Deep, BB: Barilari Bay, and MB: Marguerite Bay. (b) Surface satellite imagery and multibeam swath bathymetry of Bigo Bay with the locations of cores WAP13-GC47, WAP13-BC47, and WAP13-GC45. (For interpretation of the references to colour in this figure legend, the reader is referred to the Web version of this article.)

3.1. Physical properties

MS was measured at 1 cm intervals on split half-core sections using a Bartington MS-2B susceptibility meter at Korea Polar Research Institute (KOPRI). The WC for all cores was measured at 2 cm intervals on 1 cm thick sub-samples. The WC was calculated by the following equation:

$$WC\ (\%) = \left(\frac{Mass_{wet} - Mass_{dry} - Mass_{salt}}{Mass_{wet}}\right) \times 100$$

where $Mass_{wet}$, $Mass_{dry}$, and $Mass_{salt}$ are the mass of the original sample, dried sample, and salt (assuming 35 psμ), respectively.

3.2. Geochemical proxies

Geochemical proxies for all cores were measured at 4 cm intervals on 1 cm thick sub-samples. The biogenic silica (Si_{BIO}) concentration was measured through two methods: the wet alkaline extraction method modified from DeMaster (1981) at Pusan National University, and using a Continuous Flow Analyzer (SKALAR SAN^{plus} Analyzer) with the same wet-alkaline extraction method modified from DeMaster (1981) at KOPRI. The biogenic opal concentration was calculated by multiplying the biogenic silica concentration by 2.4 (Mortlock and Froelich, 1989). The relative error of the biogenic silica concentration in sediment samples is less than 1%. The biogenic silica concentration was measured only on core WAP13-GC47. The total inorganic carbon (TIC) concentration was measured using the UIC CO_2 coulometer (Model CM5240) at KOPRI. The $CaCO_3$ concentration was calculated by multiplying the TIC concentration by 8.333. The relative standard deviation for the $CaCO_3$ concentration is ±1%. The total carbon (TC) and total nitrogen (TN) concentrations were measured with an Organic Elemental Analyzer (FLASH, 2000 NC Analyzer) at KOPRI. The analytical precisions are better than ±0.1% and ±0.02%, respectively. The TOC concentration equals the difference between the TC and TIC.

3.3. Bulk $\delta^{15}N$ values

The bulk $\delta^{15}N$ values for core WAP13-GC47 were measured at 4 cm intervals using the EA–IRMS (Europa Scientific RoboPrep-CN elemental analyzer & Europa Scientific 20-20 mass spectrometer) at Iso-Analytical Ltd., UK. Nitrogen isotope ratios are expressed in conventional delta notation, which is the per mil deviation from atmospheric nitrogen. The precision for nitrogen isotopes was approximately ±0.2‰.

3.4. Diatom assemblage analysis

Diatom assemblages for core WAP13-GC47 were analyzed at 20 cm intervals. The detailed sample preparation and diatom counting method followed those described in Bak et al. (2007). The quantitative analysis of diatom slides followed the procedures described in Scherer (1994). The absolute abundance was calculated by the following equation:

$$Abundance = \frac{((A \times B)/(C \times D))}{E}$$

where A is the number of specimens counted, B is the settling chamber area, C is the microscope's field of view number, D is the field of view area, and E is the sample mass. *Chaetoceros* resting spores were not included in the specimen count.

3.5. Radiocarbon dating

Fifteen accelerator mass spectrometry (AMS) ^{14}C dates were measured at Beta Analytic, USA (Table 1). We analyzed nine

Table 1
Radiocarbon dates from cores WAP13-GC47 and WAP13-GC45. The calibration program CALIB 7.1 (Stuiver and Reimer, 1993; Reimer et al., 2013) was used to convert the ^{14}C ages to calendar ages with a reservoir correction of 1390 years (△R = 990 years) for shell fragments and 1570 years (△R = 1170 years) for AIOM. AIOM: acid insoluble organic matter. *Ages not included in the age model in this study.

Depth (cm)	Analyzed material	Lab code	^{14}C age (yr BP)	Error (yr)	AIOM: calibration age (σ2) △R = 1170 Shell: calibration age (σ2) △R = 990		Median Calendar age (cal. yr BP)
					cal. yr BP (min)	cal. yr BP (max)	
WAP13-GC47							
0	AIOM	Beta-364186	1670	±30	40	236	120
62	AIOM	Beta-364187	2890	±30	1209	1343	1275
80	AIOM	Beta-447357	3100	±40	1369	1582	1477
100	AIOM	Beta-447358	2900	±30	1221	1349	1283
120	AIOM	Beta-447359	3110	±30	1391	1572	1490
166*	AIOM	Beta-364188	6280	±40	5378	5572	5481
282*	Shell fragment	Beta-361570	9050	±40	8406	8606	8512
306*	AIOM	Beta-361570	8820	±40	7995	8200	8105
309*	Shell fragment	Beta-364189	8730	±30	8136	8308	8215
366	AIOM	Beta-364190	4650	±30	3265	3443	3364
514	AIOM	Beta-364191	6970	±40	6122	6299	6225
WAP13-GC45							
78*	AIOM	Beta-447360	4940	±30			
78	Scaphopod	Beta-354400	1660	±30	261	406	317
481*	AIOM	Beta-447361	5540	±30			
481	Shell	Beta-354401	2360	±30	820	993	918

horizons for acid insoluble organic matter (AIOM) and two calcareous shell fragments (at 282 cm and 309 cm) for AMS ^{14}C dates at core WAP13-GC47. In addition, we analyzed both AIOM and calcareous shell fragments at the same intervals (78 cm and 481 cm) for AMS ^{14}C dates at core WAP13-GC45.

4. Age model

Radiocarbon age results were calibrated using CALIB 7.1 (Stuiver and Reimer., 1993) with the MARINE13 dataset that includes a standard global 400 year reservoir age (R) (Reimer et al., 2013). To account for spatially and temporally variable reservoir ages, a reservoir age calibration (ΔR) was applied (Cook et al., 2005b). As a result, different ΔR values, ranging from 480 to 990 years, have been applied to radiocarbon chronologies in sediment cores from the AP (e.g., Domack, 1992; Berkman and Forman, 1996; Domack et al., 2005; Hillenbrand et al., 2010; Christ et al., 2015). We used a ΔR of 990 years (which equals a total local reservoir age of 1390 years), which was applied to the cores collected from Barilari Bay, the adjacent fjord to the south of Bigo Bay (Christ et al., 2015), for two shell fragment AMS ^{14}C dates of core WAP13-GC47.

AIOM AMS ^{14}C dates of core tops are commonly older than the local reservoir age in Antarctica due to the influence of old carbon (e.g., Gordon and Harkness, 1992; Domack et al., 2003; Hillenbrand et al., 2010). The core top AIOM age of 1670 ^{14}C yr BP (Table 1) is 280 years older than the local reservoir age (1390 year) used in this study. To determine if the core top AIOM ^{14}C age is representative of the sediment-water interface, we compared the MS, WC, and TOC concentrations between cores WAP13-GC47 and WAP13-BC47 that were collected from the same location. Based on these comparisons (Fig. S1), the upper ~5 cm of sediment from core WAP13-GC47 was lost during the coring process. Extrapolating the linear sedimentation rate between 0 cm (1670 ^{14}C yr BP) and 62 cm (2890 ^{14}C yr BP) of 0.051 cm/^{14}C yr, the lost 5 cm of core WAP13-GC47 was calculated to represent only ~100 years. The actual core top age for core WAP13-GC47 is then considered to be 1570 ^{14}C yr BP, only 180 years older than the local reservoir age of 1390 in Barilari Bay. This 180 year difference can be attributed to bioturbation, local reservoir differences, or the effect of old carbon typical of AIOM AMS ^{14}C dates in the AP; therefore, we considered this 180 year difference for the local ΔR in Bigo Bay. Thus, we used the ΔR of 1170 year for calibration of nine AIOM ^{14}C dates of core WAP13-GC47.

Two AIOM ages at 166 cm and 306 cm and two shell fragment ages at 282 cm and 309 cm of core WAP13-GC47 were excluded from our age model because they greatly exceeded the AIOM age at 514 cm (Table 1, Fig. 2). Additionally, there are chronologically inverted layers between 62 cm and 120 cm with ages ranging from 2890 ^{14}C yr BP to 3110 ^{14}C yr BP in core WAP13-GC47 (Table 1). The age measurement errors for this layer were ±30–40 years, but the analytical errors were reported as ±200 ^{14}C yr or more from Maxwell Bay (Milliken et al., 2009). Thus, the age model for core WAP13-GC47 was constructed using a third-order polynomial equation rather than a linear interpolation (Fig. 2):

$$y = 8.84E\text{-}05x^3 - 0.056x^2 + 17.252x + 212.425$$

where y = age (cal. yr BP) and x = depth (cm), which provides an r^2 value of 0.99.

For core WAP13-GC45, we also used a ΔR of 990 years for two shell fragment AMS ^{14}C dates (72 cm and 481 cm) (Table 1). Two AIOM ^{14}C dates of core WAP13-GC45 were 3280 and 3180 years older than the ^{14}C dates of shell fragments at the same intervals. This indicates a more significant old carbon effect in the inner fjord; thus, we did not convert AIOM ^{14}C dates to calendar ages for core WAP13-GC45 in this study.

5. Results

5.1. Core WAP13-GC47

Core WAP13-GC47 is composed of four lithologic units: Unit 1 (0–160 cm), Unit 2 (160–340 cm), Unit 3 (340–550 cm), and Unit 4 (550–563 cm). Unit 4 (550–563 cm) consists of homogenous dusky yellow green (5GY 5/2), and poorly sorted mud with diatoms (Fig. S2). Unit 4 is characterized by a peak MS (*ca.* 170 × 10^{-5} SI) and relatively low WC (30–45%) (Fig. 3a and b). There is low biogenic opal concentration (<15%), TOC concentration (<0.6%), and TN concentration (<0.08%), along with high bulk δ^{15}N values and $CaCO_3$ concentration (Fig. 3c–g). Gravel and sand sized fractions were almost absent (Fig. S2). The total diatom abundance is low

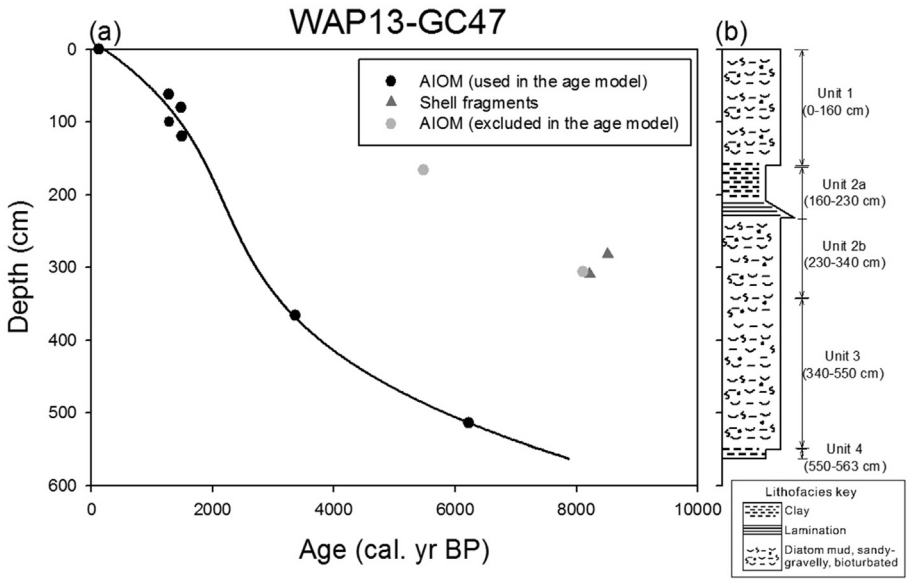

Fig. 2. (a) Third-order polynomial calibrated radiocarbon age model for core WAP13-GC47 and (b) stratigraphic column and lithofacies. Black closed circles: AIOM dates used in the age model, gray closed circles: AIOM dates (not included in the age model), and dark gray closed triangles: shell fragment dates (not included in the age model). All calibrated age are listed in Table 1.

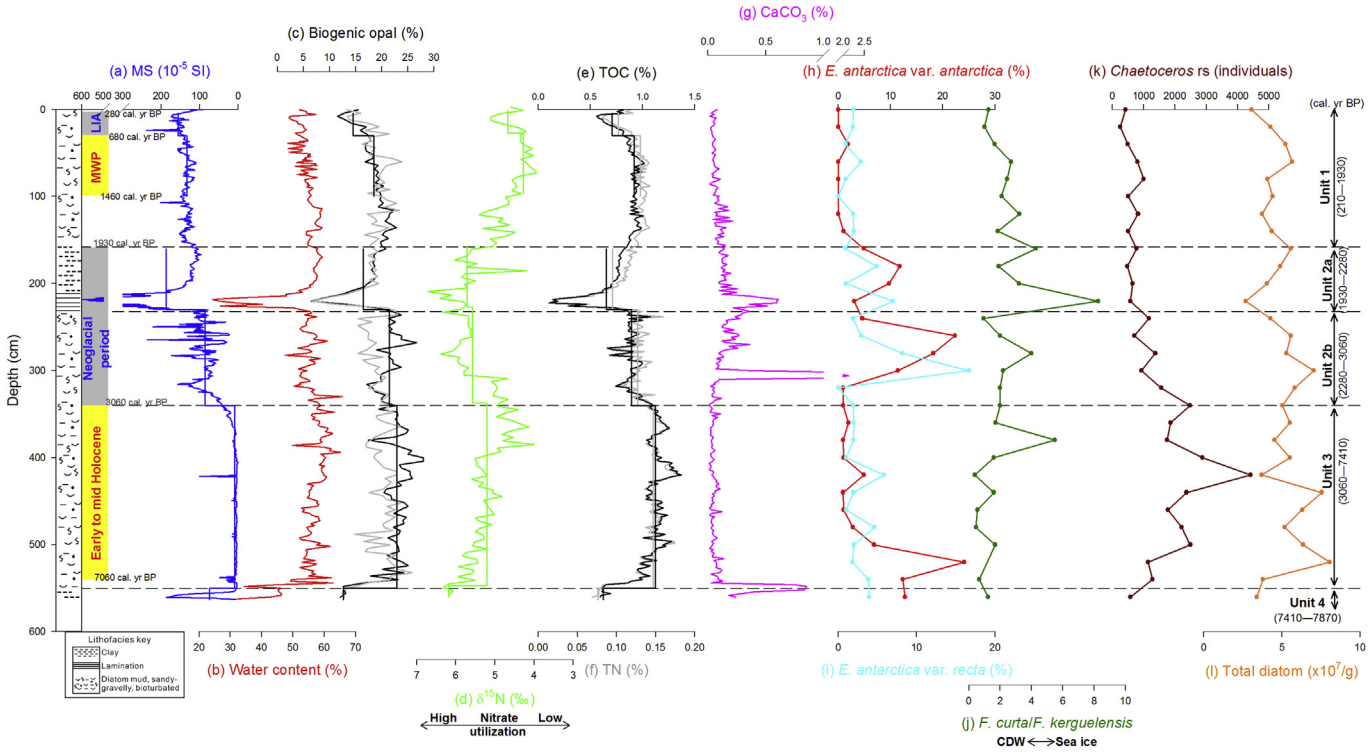

Fig. 3. WAP13-GC47 (outer fjord) downcore profiles of (a) MS, (b) WC, (C) biogenic opal concentrations (black line: measurement at KOPRI and gray line: measurement at PNU), (d) bulk $\delta^{15}N$, (e) TOC concentration, (f) TN concentration, (g) $CaCO_3$ concentration, (h) *Eucampia antarctica* var. *antarctica* (warm conditions), (i) *E. antarctica* var. *recta* (cold conditions), (j) *Fragilariopsis curta*/*F. kerguelensis* ratio, (k) abundance of *Chaetoceros* resting spores, and (l) total diatom abundance. Straight lines in (a), (c), (d), (e), and (f) are unit average values.

with low counts of *Chaetoceros* resting spores, a low *Fragilariopsis curta*/*F. kerguelensis* ratio, high *Eucampia antarctica* var. *antarctica*, and relatively low *E. antarctica* var. *recta* (Fig. 3h–l).

Unit 3 (340–550 cm) consists of moderately olive brown (5Y 4/4) to light olive (10Y 5/4), bioturbated diatomaceous poorly sorted mud and diatom ooze (Fig. S2). Unit 3 is characterized by low MS (generally lower than 10×10^{-5} SI), and relatively high WC (55–60%). The biogenic opal concentrations are high (20–25%) as are the TOC and TN concentrations (1–1.4% and 0.13–0.17%, respectively) (Fig. 3c, e, and f). Unit 3 has low bulk $\delta^{15}N$ (5.2‰ in average) values and $CaCO_3$ concentrations (Fig. 3d and g). The total diatom abundance is relatively high, including high *Chaetoceros*

resting spores (>2000 counts) with low *F. curta*/*F. kerguelensis* ratio (<2) (Fig. 3j–l). *E. antarctica* var. *antarctica* was high (*ca.* 25%) at 520 cm, then decreased significantly, whereas *E. antarctica* var. *recta* was relatively low (*ca.* 2.5% in average) with small variations (Fig. 3h and i).

Unit 2 (160–340 cm) consists of two sub-units: Unit 2a, a dusky yellow green (5GY 5/2), upward fining turbidite sequence with faint laminations that overlies interbedded laminated sand and mud (160–230 cm), and Unit 2b, a light olive (10Y 5/4) to grayish olive (10Y 4/2), bioturbated, diatom-bearing mud with sparse bioclasts (230–340 cm) (Fig. S2). Unit 2 is characterized by the highest sedimentation rates (*ca.* 160 cm/kyr on average) (Fig. 2), relatively high MS values (generally lower than 120×10^{-5} SI but reach 600×10^{-5} SI at the laminated layer, 210–230 cm), and moderate WC (50–60%) that declines to 25% at the laminated layer (Fig. 3a and b). The biogenic opal concentration varies from relatively high to low (15–25%) and moderate TOC and TN concentrations (0.8–0.9% and 0.12–0.13%, respectively) with minimum values of 5%, 0.1%, and 0.01% at the laminated layer, respectively (Fig. 3c, e, and f). The bulk $\delta^{15}N$ values and $CaCO_3$ concentration are relatively high (Fig. 3d and g). Unit 2b has gravel-sized grains but Unit 2a has no gravel-sized grains (Fig. S2). The total diatom abundance is moderate with decreasing *Chaetoceros* resting spores upward from 340 cm and relatively high abundance of both *E. antarctica* var. *antarctica* and *E. antarctica* var. *recta* and high ratio of *F. curta*/*F. kerguelensis* ratio (>2) (Fig. 3h–l).

Unit 1 (0–160 cm) consists light olive (10Y 5/4), bioturbated, diatom-bearing, poorly sorted mud (Fig. S2). Unit 1 is characterized by high MS ($100–170 \times 10^{-5}$ SI), moderate WC (50–60%), relatively high biogenic opal concentrations (15–23%) and TOC and TN concentrations (0.55–1% and 0.08–0.12%, respectively) that decreases up core (Fig. 3c, e, and f). The bulk $\delta^{15}N$ values and $CaCO_3$ concentrations are low (<0.1%) (Fig. 3d and g). Unit 1 has a moderate total diatom abundance with few *Chaetoceros* resting spores. Both *E. antarctica* var. *antarctica* and *E. antarctica* var. *recta* are nearly absent from Unit 1 (Fig. 3h, i, k, and l).

Across the entire core, biogenic opal concentrations, a proxy for diatom abundance, co-vary similarly with the TOC, TN, total diatom abundance, WC, and MS (Fig. 3a–c, e, f, and l). The bulk $\delta^{15}N$ values, biogenic opal, TOC, and TN concentrations generally co-vary (Fig. 3c–f). The $CaCO_3$ concentrations are generally very low (<0.1%) but show a positive relationship with the MS (Fig. 3a and g). The biogenic opal concentration measured at KOPRI correlated more strongly with the other proxies described above, but our interpretations remain similar regardless of which biogenic opal method was used for core WAP13-GC47.

5.2. Core WAP13-GC45

Core WAP13-GC45 is composed of bioturbated dark greenish gray (5GY 4/1) sandy mud intercalated with frequent sandy lamina. Core WAP13-GC45 corresponds to Unit 1 of core WAP13-GC47 and is characterized by a similar level of MS ($100–200 \times 10^{-5}$ SI), lower WC (30–40%) and TOC and TN concentrations (<0.5% and <0.06%, respectively), and higher $CaCO_3$ concentration (0.4% in average) (Fig. 4).

6. Discussion

Our multi-proxy dataset allows us to reconstruct a Holocene paleoenvironmental history of outer Bigo Bay: early Holocene cooling (*ca.* 8500–7060 cal. yr BP), seasonally open marine conditions in the warmer early to mid-Holocene (*ca.* 7060–3060 cal. yr BP), followed by variations in sea ice coverage and possible glacial advance that corresponds to Neoglacial cooling (*ca.* 3060–1930 cal. yr BP), MWP warming (*ca.* 1460–680 cal. yr BP), and LIA cooling (*ca.* 680–280 cal. yr BP). With this paleoenvironmental record, we draw connections between surface water productivity and nutrient utilization in WAP fjords and the implications for surface-deep water mass exchange.

6.1. Early Holocene deglaciation patterns

Following deglaciation, seasonally open marine conditions prevailed during the early and middle Holocene in the WAP (Allen et al., 2010; Christ et al., 2015). Unit 4 (550–563 cm) is a homogenous dusky yellow green (5GY 5/2) mud with diatoms and no gravel-sized grains. Silty clay (mud) with low indicators of primary productivity, similar to the characteristics of Unit 4 in core WAP13-GC47, may indicate a sub-ice shelf setting (Domack et al., 1999, 2003). Above the mud unit, high biogenic opal, TOC, TN concentrations occurred in Unit 3 with the common appearance of gravel-sized grains, indicating a shift from sub-ice shelf settings (Unit 4) to seasonally open marine conditions (Unit 3) as the calving line retreated.

Proxies indicative of enhanced primary productivity, and thus seasonally open marine conditions, characterize the bottom of Unit 3 (*ca.* 540 cm): increased biogenic opal, TOC, and TN concentrations, and WC, and decreased MS values (Fig. 3a–c, e, and f). Seasonally open marine conditions are further suggested by increased total diatom abundance, especially abundant *Chaetoceros* resting spores, and *E. antarctica* var. *antarctica* (Fig. 3h, k, and l), a diatom species indicative of the warm early Holocene following the last deglaciation in the Palmer Deep (*ca.* 9000 and 6700 cal. yr BP; Leventer et al., 2002). Thus, 540 cm depth corresponds to *ca.* 7060 cal. yr BP and is consistent with sedimentary characteristics of the onset of seasonally open marine conditions from cores collected elsewhere in the WAP (e.g., Taylor et al., 2001; Leventer et al., 2002; Bentley et al., 2005; Allen et al., 2010) as well as a record of ice sheet retreat deduced from lake sediments in Marguerite Bay (Hodgson et al., 2013).

Due to the presence of shell fragments with ages (8215 cal. yr BP at 309 cm and 8512 cal. yr BP at 282 cm) far older than the surrounding matrix (2800–2600 cal. yr BP) in Unit 2b, we infer retreated glacial positions in Bigo Bay during the early Holocene. We interpret that these older shell fragments were deposited during the earliest Holocene in the inner fjord of Bigo Bay, and then transported to outer Bigo Bay, possibly by a glacial advance during the Neoglacial period (e.g., Hansom and Flint, 1989; Hall et al., 2010; Christ et al., 2015). Weak glacial lineations seaward of the present Comrie Glacier front visible on the multibeam bathymetry data suggest geomorphic evidence for advanced glacial positions in the recent geologic past (Fig. 1b). Unit 2b (230–340 cm) of core WAP13-GC47 is characterized by an increasing trend of MS with very high sedimentation rates, which also supports that this layer was laterally transported from shallower inner fjord (Fig. 2 and fig. S2).

Retreated glacial position under warm conditions during the early Holocene is also supported by the abundant occurrence of warm early Holocene indicative species, *E. antarctica* var. *antarctica* in Unit 2b (Fig. 3h). Thus, Bigo Bay was seasonally open once at least *ca.* 8500 cal. yr BP. In Barilari Bay, the adjacent fjord to the south of Bigo Bay, the onset of seasonally open marine conditions occurred at least 7022 cal. yr BP (Christ et al., 2015). The age of shell fragments at core WAP13-GC47 and characteristics of Unit 4 suggest that this area of the WAP transitioned to seasonally open marine conditions at least 8500 cal. yr BP and cooled again some time before *ca.* 7060 cal. yr BP. Warmer conditions between 9.7 and 7.0 cal. yr BP were reported from Marguerite Bay, WAP (Peck et al., 2015). The consistent and inconsistent points between Bigo and

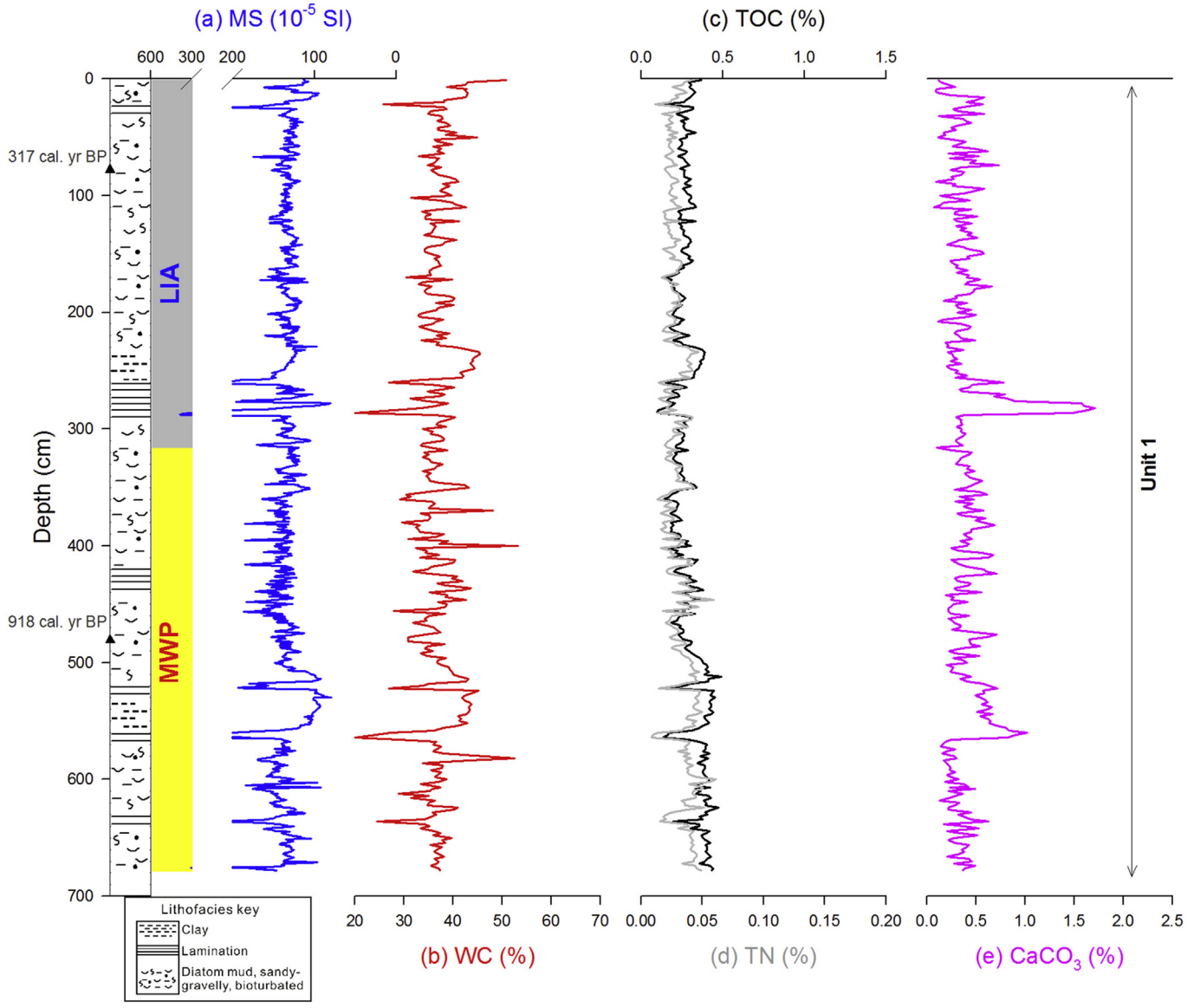

Fig. 4. WAP13-GC45 (inner fjord) downcore profiles of (a) MS, (b) WC, (C) TOC concentration, (d) TN concentration, and (e) $CaCO_3$ concentration.

Marguerite Bays suggest both regions became open marine conditions, but Bigo Bay underwent cooling conditions showing regionally different behaviors in the WAP.

Although an early Holocene climate cooling has not been commonly reported from previously analyzed sediment cores in the WAP (e.g., Domack et al., 1995, 2003; Allen et al., 2010; Hillenbrand et al., 2010; Christ et al., 2015; Peck et al., 2015), other evidence exists in the AP. On the eastern side of the AP, on James Ross Island (JRI), outcrops of glacial sediments near the coast indicated glacial re-advance from 7.6 to 7.3 cal. yr BP (Strelin et al., 2006). Following the early Holocene optimum, the JRI ice core records climate stabilization after 8000 yr BP (Mulvaney et al., 2012). In the southwest AP, the George VI Ice Shelf was absent *ca.* 9595 cal. yr BP but reformed by *ca.* 7945 cal. yr BP (Bentley et al., 2005). Taken together, these datasets highlight the spatial and temporal complexity of (de)glaciation in the AP during the early Holocene. Thus, further studies on the early Holocene glacial advance/cooling in the WAP are necessary to understand the pattern of deglaciation in the WAP.

6.2. Early to mid-Holocene (ca. 8500–3060 cal. yr BP)

Unit 3 of core WAP13-GC47 (340–550 cm; *ca.* 7410–3060 cal. yr BP) is characterized by low MS, high biogenic opal, TOC, and TN concentrations, WC, low ratio of *F. curta*/*F. kerguelensis*, and high abundance of *Chaetoceros* resting spores (Fig. 3a–c, e, f, j, and k). These characteristics correspond to seasonally open marine conditions during the warm mid-Holocene in the WAP (e.g., Domack et al., 1995, 2003; Leventer et al., 1996; Shevenell et al., 1996; Taylor et al., 2001; Allen et al., 2010; Christ et al., 2015). At *ca.* 7060 cal. yr BP *E. antarctica* var. *antarctica* was abundant (Fig. 3h). Meltwater from glaciers and icebergs delivers iron to surface water and promotes production of *E. antarctica* var. *antarctica* (Burckle, 1984; Smith et al., 2007b; Armand et al., 2008). During deglaciation in the early Holocene elsewhere in the WAP, such as Marguerite Bay and other coastal fjords, enhanced meltwater production afforded more favorable conditions for *E. antarctica* var. *antarctica* (Allen et al., 2010). Thus, the diatom assemblage shift from *E. antarctica* var. *antarctica* to *Chaetoceros* resting spores may

correspond to a warmer climate during the early to mid-Holocene in Bigo Bay (Fig. 3h and k). The co-variation between biogenic opal and TOC concentrations confirms that diatom production reflects surface water production in the WAP. Elsewhere in the WAP during the mid-Holocene, high surface water productivity corresponds to reduced sea ice cover and prolonged growing seasons (Domack et al., 1995, 2003; Leventer et al., 1996; Taylor et al., 2001; Brachfeld et al., 2003; Allen et al., 2010). This is supported by the low ratio of *F. curta*/*F. kerguelensis* (Fig. 3j), which is a proxy for sea ice coverage (Peck et al., 2015 and references therein). Although nutrient availability is one of major factors for controlling surface water productivity, nutrient utilization changes in response to surface water productivity changes have been poorly investigated in the inner shelf area of the WAP.

Bulk $\delta^{15}N$ values can reflect changes in the extent of nitrate consumption in the surface water (Francois et al., 1992; Altabet and Francois, 1994). Although bulk $\delta^{15}N$ values are related to nitrate utilization by phytoplankton in the euphotic zone (Robinson and Sigman, 2008), the co-variation of biogenic opal and TOC and TN concentrations indicates that diatoms are the dominant species that regulate surface water productivity in Bigo Bay (Fig. 3c, e, and f). Decreased $\delta^{15}N$ values, indicating lower nitrate utilization, coincide with high surface water productivity during the mid-Holocene at core WAP13-GC47 (Fig. 3c and d). Reduced nitrate utilization and enhanced surface productivity at high latitudes in both the northern and southern hemispheres may result from stronger upwelling of nutrient-rich deep waters (e.g., Brzezinski et al., 2002; Brunelle et al., 2007, 2010; Studer et al., 2015). Significant upwelling and intrusion of the CDW onto the continental shelf of the WAP occurred during the mid-Holocene (Leventer et al., 2002; Allen et al., 2010), providing a potential mechanism to explain the low bulk $\delta^{15}N$ and high surface water productivity values in Unit 3 of core WAP13-GC47.

Chaetoceros resting spores can indicate surface water stratification in association with a receding ice edge (Leventer et al., 1996; Sjunneskog and Taylor, 2002), which seemingly contradicts our bulk $\delta^{15}N$ value-based and surface water productivity-based interpretation of mid-Holocene paleoenvironment. However, *Chaetoceros* resting spores were not abundant under favorable conditions confirmed by other diatom assemblages (Sjunneskog and Winter, 2012). In addition, *Chaetoceros* resting spores may also be associated with upwelling water masses such as CDW (Sjunneskog and Winter, 2012). The low ratio of *F. curta*/*F. kerguelensis* at core WAP13-GC47 also supports less sea ice and more open marine conditions (Fig. 3k). Since sea ice coverage and duration decreases under warmer climates in the WAP (Taylor et al., 2001; Gersonde et al., 2005; Allen et al., 2010), we can expect a similarly short duration of surface water stratification. Thus, high surface water productivity with low nitrate utilization during the mid-Holocene is related to decreased sea ice meltwater input and strong CDW upwelling.

6.3. Neoglacial period (ca. 3060–1930 cal. yr BP)

At *ca*. 3060 cal. yr BP, the MS values and $CaCO_3$ began to increase in core WAP13-GC47 (Fig. 3a and g). The MS values, usually related to terrestrial material input (Leventer et al., 1996), increase with proximity to the grounding line in Barilari Bay (Christ et al., 2015). The MS increase with more gravel-sized grains and sandy to silty sand laminae suggests a possible glacial advance via meltwater plumes and iceberg calving within Bigo Bay, as shown elsewhere in the WAP. Reworked shell fragments and sediments in Unit 2b (*ca*. 3060–2280 cal. yr BP) indicate that there was lateral transport from the inner fjord with a glacial advance. The $CaCO_3$ concentrations are very low, but clearly increase in step with the MS values under glacial advance (Fig. 3a and g). Thus, increases in $CaCO_3$ concentration potentially provide evidence for sediment reworking from inner fjords related to glacial advance in the WAP.

The timing of the Neoglacial cooling and inferred glacial advance in Bigo Bay corroborates observations across many sites in the WAP that initiated between 3500 and 2500 cal. yr BP (Leventer et al., 1996; Domack et al., 2001, 2003; Taylor et al., 2001; Milliken et al., 2009; Allen et al., 2010; Christ et al., 2015). Recently, it was reported that enhanced sea ice coverage, based on the high *F. curta*/*F. kerguelensis* ratio, started from *ca*. 4000 cal. yr BP in Marguerite Bay, WAP (Peck et al., 2015). The *F. curta*/*F. kerguelensis* ratio at core WAP13-GC47 increased *ca*. 3500 cal. yr BP (380 cm), which is earlier than the timing (3060 cal. yr BP) based on other proxies (Fig. 3). This finding suggests that the spatial difference of climatic events in the WAP may be derived from using different proxies. Both *E. antarctica* var. *recta*, a proxy for colder conditions, and *E. antarctica* var. *antarctica*, a proxy for warm conditions (Fryxell and Prasad, 1990; Fryxell, 1991; Leventer et al., 2002), co-occur in core WAP13-GC47 during the Neoglacial period (Fig. 3h and i), similar to observations in Lallemand Fjord (Taylor et al., 2001). Ages of shell fragments found in this layer correspond to the early Holocene time period, requiring transport from the inner to outer Bigo Bay, possibly via glacial advance and subsequent deposition from a meltwater plume or ice rafting, after *ca*. 3060 cal. yr BP. Furthermore, species associated with colder conditions were deposited at outer Bigo Bay during the Neoglacial period. This is consistent with the interpretation that Unit 2a (160–230 cm) is composed of mixed sediments; some are transported from the inner fjord and some are deposited at outer Bigo Bay.

A turbidite layer overlying a sandy to silty sand laminae occurs at in Unit 2a (210–230 cm) of core WAP13-GC47. Although lamination may form via meltwater input (e.g., Shevenell et al., 1996), we interpret the glacier proximal deposition for the laminated layer in core WAP13-GC47 shown by MS and $CaCO_3$. Similar to Barilari Bay, the advance of the grounding line in the inner fjord of Bigo Bay may have triggered small submarine landslides and subsequent turbidity currents at the edge of the grounding zone wedge seaward of the Comrie Glacier (Christ et al., 2015). We interpret the turbidite layer in core WAP13-GC47 as indirect evidence for glacial advance during the Neoglacial period in Bigo Bay. Gravel-sized grains were not found in the 210–160 cm turbidite interval at core WAP13-GC47 (Fig. S2), suggesting rapid deposition, which is supported by the high sedimentation rates of this interval (Fig. 2). Outer Bigo Bay, as was observed at Barilari Bay, was likely not covered by an ice shelf during the Neoglacial period, as TOC, TN, biogenic opal concentrations, WC, and total diatom abundance were not extremely low (Fig. 3b, c, e, f, and l) (e.g., Shevenell et al., 1996; Christ et al., 2015).

Unit 2 is characterized by increased bulk $\delta^{15}N$ values (5.6‰ on average with maximum value of 6.5‰) and decreases in biogenic opal, TOC, and TN concentrations, WC, and total diatom abundance, though not by much (Fig. 3b–f and k). This indicates enhanced nitrate utilization without significant reduction in surface water productivity at core WAP13-GC47. Unit 2 is also characterized by abundant *E. antarctica* var. *recta*, indicating cold conditions, and high ratios of *Fragilariopsis curta*/*F. kerguelensis*, indicating sea ice dominant conditions (Peck et al., 2015 and references therein). The nitrogen isotopic epsilon of sea ice diatoms and open water diatoms differ (Horn et al., 2011), as well as the diatom assemblage between the mid-Holocene and Neoglacial period (Taylor et al., 2001; Allen et al., 2010; this study). However, this previous diatom culture experiment was not performed under species' natural habitat conditions and did not use diatom species in the WAP. Diatom-bound $\delta^{15}N$ values of total diatom species were used as a proxy

for nitrate utilization in spite of the $\delta^{15}N$ differences between pennate and centric types (Studer et al., 2015). In addition, the bulk $\delta^{15}N$ values reflect changes in the extent of nitrate consumption in the surface water by phytoplankton communities (Francois et al., 1992; Altabet and Francois, 1994). Thus, we interpreted changes in bulk $\delta^{15}N$ values as utilization changes in this study, despite the potential influence of diatom assemblage changes on bulk $\delta^{15}N$ values.

Increased bulk $\delta^{15}N$ values during the Neoglacial period can be associated with nitrate utilization changes in response to enhanced sea ice coverage that results in more sea ice meltwater discharge (Shevenell et al., 1996; Taylor et al., 2001; Allen et al., 2010). Previous studies have linked extensive sea ice coverage and associated light inhibition with reduced surface water productivity during the Neoglacial period in the WAP (e.g., Shevenell et al., 1996; Sjunneskog and Taylor, 2002; Domack et al., 2003; Christ et al., 2015). If light inhibition associated with extensive sea ice is the dominant factor for controlling surface water productivity (e.g., Ingólfsson et al., 1998; Allen et al., 2010), lower nitrate utilization is expected. In contrast, nitrate utilization enhanced at outer Bigo Bay during the Neoglacial period. Panizzo et al. (2014) suggested that enhanced nutrient utilization is in isolated sea ice but corresponds to less than 1% of total carbon budgets beneath the sea ice in the Arctic Ocean (Lee et al., 2015). Although a similar total carbon budget in the Antarctic region does not yet exist, it suggests that production in sea ice does not control bulk $\delta^{15}N$ values. Sea ice meltwater enhances stratification (Mitchell and Holm-Hansen, 1991; Meredith et al., 2010) and supplies micronutrients (Meredith et al., 2010), leading to enhanced nitrate utilization. Thus, our results suggest that during cold periods, increased sea ice meltwater input and a shorter growing season led to enhanced nitrate utilization and afforded relatively high surface productivity.

6.4. Medieval Warm Period (ca. 1460–680 cal. yr BP)

Enhanced productivity under more oceanic conditions in the Palmer Deep from 1150 to 700 cal. yr BP marks the Medieval Warm Period (MWP) (Domack et al., 2003). Although the $\delta^{13}C$ of organic matter in the outer fjord of Barilari Bay increased between 1325 and 626 cal. yr BP (Christ et al., 2015), robust evidence for the MWP event was not observed. Biogenic opal, TOC, and TN concentrations only increased slightly without coeval increases in WC or decreases in MS after *ca.* 1930 cal. yr BP in core WAP13-GC47 (Fig. 3a–c, e, and f). The MS values are even slightly increased compared to the beginning of the Neoglacial period (Fig. 3a). Similarly, only the TOC and TN concentrations of core WAP13-GC45 (inner fjord) slightly increased before 918 cal. yr BP (Fig. 4c and d). However, bulk $\delta^{15}N$ values decrease upcore from 160 cm (*ca.* 1930 cal. yr BP), with notably low values between 30 and 100 cm (*ca.* 1460–680 cal. yr BP) (Fig. 3d). This possibly indicates reduced nitrate utilization due to weaker surface water stratification via less sea ice melt under warmer climates. This is supported by high TEX_{86} sea surface temperatures (2.9 °C in average) in Palmer Deep during 1600 to 500 cal. yr BP (Shevenell et al., 2011). Thus, the record of *ca.* 1460–680 cal. yr BP at Bigo Bay most likely corresponds to the MWP event and climatic warmth that may have initiated *ca.* 1930 cal. yr BP in the WAP, although the signal is not very clear. The MWP is more easily recognized through the bulk $\delta^{15}N$ or $\delta^{13}C$ of organic matter, rather than productivity-related proxies in the WAP and is due to very poor preservation of opal and TOC (Chase et al., 2015 and references therein). These isotopic proxies may record more subtle changes in climatic and oceanic conditions better than other productivity proxies in the WAP.

6.5. Little Ice Age (ca. 680–280 cal. yr BP)

Between 4 and 30 cm (*ca.* 680–280 cal. yr BP), the MS increased, and WC, biogenic opal, TOC, and TN concentrations, and total diatom abundance decreased (Fig. 3a–c, e, f, and l), indicating reduced surface water productivity. Although the timing of the LIA event in the WAP widely ranges (e.g., Allen et al., 2010; Christ et al., 2015 and references therein), these results confirm observations of a Late Holocene cooling in the WAP (e.g., Shevenell et al., 1996; Taylor et al., 2001; Shevenell et al., 2011; Christ et al., 2015). The LIA glacial advance and ice shelf expansion in Barilari Bay are marked by a fluted grounding zone wedge composed of diamict in the inner fjord, interbedded laminated mud and sandy turbidites with extremely low %TOC and primary productivity below an ice shelf in the middle fjord, and increased fine terrigenous sediment input and depressed primary productivity under ice shelf proximal or fast-ice conditions in the outer fjord (Christ et al., 2015).

Our results from core WAP13-GC47 in outer Bigo Bay confirm reduced surface water productivity during the regional LIA event. Similar to outer Barilari Bay, fine-grained terrigenous sedimentation increases with gravel-sized grains, and primary productivity proxies (biogenic opal and TOC concentrations and total diatom abundance) decrease. This decline in primary productivity could be attributed to expansion of an ice shelf into the outer fjord, greatly enhanced sea ice coverage, or both between *ca.* 680 and 280 cal. yr BP. We cannot directly infer glacial advance, nor ice shelf expansion, from core WAP13-GC47 because it was collected from the outer fjord. The possible presence of a fluted grounding zone wedge seaward of Comrie Glacier (Fig. 1b) and the decay of a remnant ice shelf in the small alcove in northern Bigo Bay (Ferrigno et al., 2008), however, suggests a recent, prehistoric glacial advance event in Bigo Bay that was potentially contemporaneous with glacial advance and ice shelf growth in adjacent Barilari Bay (Christ et al., 2015). Compared to Barilari Bay, fewer and smaller glaciers drain into Bigo Bay that contains multiple shallow (<50 m deep) areas and islands. The late Holocene advance of the Comrie Glacier and a floating ice tongue could have pinned onto these shallow areas to form a fjord-wide ice shelf.

In the inner fjord, core WAP13-GC45 is characterized by decreased TOC and TN concentrations from the MWP to the LIA, low water content, and the occurrence of sandy laminations during the LIA. Core WAP13-GC45 is composed of mud with low productivity during the LIA, indicating sub-ice shelf setting. Sandy laminae along with low WC, TOC and TN concentrations, and high MS and $CaCO_3$ at the beginning of the LIA (260–290 cm) suggests deposition via meltwater pulsing and proximity to the grounding line in the inner fjord of Bigo Bay (Fig. 4). The $CaCO_3$ increase at 550 cm at core WAP13-GC45 may suggest glacial advance in the inner fjord (Fig. 4e).

The bulk $\delta^{15}N$ values are lower than those observed during the Neoglacial period, however, they show relatively increased values (*ca.* 5.6‰) (Fig. 3d). Likewise, in the Neoglacial period, increased nitrate utilization may reflect enhanced stratification from increased sea ice meltwater flux. Surface water stratification could also result from meltwater sourced from an advanced ice shelf calving front in outer Bigo Bay, similar to Barilari Bay, during the LIA (Christ et al., 2015). Although the influence of meltwater sourced from the calving front on outer Bigo Bay during the LIA cold period remains unknown, it cannot be excluded as a cause of surface stratification in outer Bigo Bay, because meltwater from the sea ice and ice shelf calving front may cause similar surface stratification. The $CaCO_3$ increase from 550 cm at core WAP13-GC45 may suggest glacial advance in the inner fjord (Fig. 4e). In addition, the presence of gravel-sized grains indicates ice berg calving in outer Bigo Bay (Fig. S2).

7. Conclusions

We compiled a multi-proxy dataset (MS, WC, concentrations of biogenic opal, TOC, TN, and $CaCO_3$, bulk $\delta^{15}N$, and diatom assemblage) to reconstruct Holocene paleoenvironmental changes in Bigo Bay, WAP, with a particular emphasis on the relationship between nutrient utilization, surface water productivity, sea ice duration and extent, and CDW upwelling. The chronological contrast between shell fragment age (ca. 8500 cal. yr BP) in Unit 2 and open marine conditions (7060 cal. yr BP) suggests that following the LGM, Bigo Bay deglaciated by at least 8500 cal. yr BP in the earliest Holocene and completed by 7060 cal. yr BP with a cooling event in between. The warm mid-Holocene and MWP were characterized by high surface water productivity with low nitrate utilization, whereas the cold Neoglacial period and LIA were characterized by relatively lower productivity with high nitrate utilization in the WAP. These variations in nitrate utilization reflect spatio-temporal variability in sea ice coverage and/or the position of an ice shelf calving front that stabilizes surface water, supplies micronutrient through melting, and supplies macronutrients through CDW input in the WAP. Although during cold periods enhanced stratification via increased sea ice meltwater and meltwater sourced from the advanced calving front may maximize nitrate utilization, surface water productivity decreased due to a nutrient supply decrease by weak CDW upwelling in the WAP. Our multi-proxy records suggest that there is a close linkage between surface water productivity, nutrient supply/utilization, surface-deep water exchange, sea ice, and glacial advance/retreat in Bigo Bay, WAP during the Holocene.

Acknowledgements

We would like to thank the crew and scientific party of the R/V *Araon* for all their help during the gravity coring on board. We would like to thank KOPRI laboratory members for all their help during experimental measurements. We appreciate the handling editor (Dr. Ingrid Hendy) and two anonymous reviewers for their critical and constructive comments to improve data interpretation and manuscript structure. This research was supported by KOPRI project (PE18030). Finally, we would like to pay our deepest respects to our late colleague, Eugene Domack. He was an excellent and enthusiastic scientist who was dedicated to mentoring young scientists and collaborating with his many colleagues across the globe, all in the pursuit of expanding scientific knowledge. Rest in peace, Gene.

Appendix A. Supplementary data

Supplementary data related to this article can be found at https://doi.org/10.1016/j.quascirev.2018.05.028.

References

Ainley, D.G., Jacobs, S.S., 1981. Sea-bird affinities for ocean and ice boundaries in the Antarctic. Deep Sea Res. 28, 1173–1185.

Allen, C.S., Oakes-Fretwell, L., Anderson, J.B., Hodgson, A., 2010. A record of Holocene glacial and oceanographic variability in Neny fjord, antarctic Peninsula. Holocene 20, 551–564. https://doi.org/10.1177/0959683609356581.

Altabet, M.A., Francois, R., 1994. Sedimentary nitrogen isotopic ratio as a recorder for surface ocean nitrate utilization. Global Biogeochem. Cycles 8, 103–116.

Armand, L.K., Cornet-Barthaux, V., Mosseri, J., Quéguiner, B., 2008. Late summer diatom biomass and community structure on and around the naturally iron-fertilised Kerguelen Plateau in the Southern Ocean. Deep-Sea Res. II 55, 653–676.

Bak, Y.-S., Yoo, K.-C., Yoon, H.I., Lee, J.-D., Yun, H., 2007. Diatom evidence for Holocene paleoclimatic change in the south Scotia sea, west Antarctica. Geosci. J. 11, 11–22.

Bentley, M.J., Hodgson, D.A., Sugden, D.E., Roberts, S.J., Smith, J.A., Leng, M.J., Bryant, C., 2005. Early Holocene retreat of the George VI ice shelf, antarctic Peninsula. Geology 33, 173–176. https://doi.org/10.1130/G21203.1.

Bentley, M.J., Hodgson, D.A., Smith, J.A., Ó Cofaigh, C., Domack, E.W., Larter, R.D., Roberts, S.J., Brachfeld, S., Leventer, A., Hjort, C., Hillenbrand, C.D., Evans, J., 2009. Mechasisms of Holocene palaeo-environmental change in the antarctic Peninsula region. Holocene 19, 51–69. https://doi.org/10.1177/0959683608096603.

Berkman, P.A., Forman, S.L., 1996. Pre-bomb radiocarbon and the reservoir correction for calcareous marine species in the Southern Ocean. Geophys. Res. Lett. 23, 363–366. https://doi.org/10.1029/96GL00151.

Brachfeld, S., Domack, E., Kissel, C., Laj, C., Leventer, A., Ishman, S., Gilbert, R., Camerlenghi, A., Eglinton, L.B., 2003. Holocene history of the Larsen-A Ice Shelf constrained by geomagnetic paleointensity dating. Geology 31, 749–752. https://doi.org/10.1130/G19643.1.

Brunelle, B.G., Sigman, D.M., Cook, M.S., Keigwin, L.D., Haug, G.H., Plessen, B., Schettler, G., Jaccard, S.L., 2007. Evidence from diatom-bound nitrogen isotopes for subarctic Pacific stratification during the last ice age and a link to North Pacific denitrification changes. Paleoceanography 22. https://doi.org/10.1029/2005PA001205. PA1215.

Brunelle, B.G., Sigman, D.M., Jaccard, S.L., Keigwin, L.D., Plessen, B., Schettler, G., Cook, M.S., Haug, G.H., 2010. Glacial/interglacial changes in nutrient supply and stratification in the western subarctic North Pacific since the penultimate glacial maximum. Quat. Sci. Rev. 29, 2579–2590.

Brzezinski, M.A., Pride, C.J., Franck, V.M., Sigman, D.M., Sarmiento, J.L., Matsumoto, K., Gruber, N., Rau, G.H., Coale, K.H., 2002. A switch from $Si(OH)_4$ to NO_3^- depletion in the glacial Southern Ocean. Geophys. Res. Lett. 29 https://doi.org/10.1029/2001GL014349, 5–1–5-4.

Burckle, L.H., 1984. Ecology and paleoecology of the marine diatom *Eucampia Antarctica* (Castr.) mangin. Mar. Micropaleontol. 9, 77–86.

Cape, M.R., Vernet, M., Skvarca, P., Marinsek, S., Scambos, T., Domack, E.W., 2015. Foehn winds link climate-driven warming to ice shelf evolution in Antarctica. J. Geophys. Res. Atmos. 120, 11,037–11,057. https://doi.org/10.1002/2015JD023465.

Castagno, P., Falco, P., Dinniman, M.S., Spezie, G., Budillon, G., 2017. Temporal variability of the circumpolar deep water inflow onto the Ross sea continental shelf. J. Mar. Syst. 166, 37–49. https://doi.org/10.1016/j.jmarsys.2016.05.006.

Chase, Z., Kohfeld, K.E., Matsumoto, K., 2015. Controls on biogenic silica burial in the Southern Ocean. Global Biogeochm. Cycles 29, 1599–1616. https://doi.org/10.1002/2015GB005186.

Christ, A.J., Talaia-Murray, M., Elking, N., Domack, E.W., Leventer, A., Lavoie, C., Brachfeld, S., Yoo, K.-C., Gilbert, R., Jeong, S.-M., Petrushak, S., Wellner, J., the LARISSA Group, 2015. Late Holocene glacial advance and ice shelf growth in Barilari Bay, Graham land, west Antarctic Peninsula. Geol. Soc. Am. Bull. 127, 297–315. https://doi.org/10.1130/B31035.1.

Cook, A.J., Fox, A.J., Vaughan, D.G., Ferrigno, J.G., 2005a. Retreating glacier fronts on the Antarctic Peninsula over the past half-century. Science 308, 541–544. https://doi.org/10.1126/science.1104235.

Cook, A.J., Holland, P.R., Meredith, M.P., Murray, T., Luckman, A., Vaughan, D.G., 2016. Ocean forcing of glacier retreat in the western Antarctic Peninsula. Science 353, 283–286. https://doi.org/10.1126/science.aae0017.

Cook, M.S., Keigwin, L.D., Sancetta, C.A., 2005b. The deglacial history of surface and intermediate water of the Bering Sea. Deep-Sea Res. II 52, 2163–2173.

DeMaster, D.J., 1981. The supply and accumulation of silica in the marine environment. Geochem. Cosmochim. Acta 5, 1715–1732.

Dierssen, H.M., Smith, R.C., Vernet, M., 2002. Glacial meltwater dynamics in coastal waters west of the Antarctic Peninsula. P. Nati. Acad. Sci. USA 99, 1790–1795.

Domack, E.W., 1992. Modern carbon-14 ages and reservoir corrections for the Antarctic Peninsula and Gerlache Strait area. Antarct. J. U. S. 27, 63–64.

Domack, E.W., Ishman, S.E., Stein, A.B., Jull, A.J.T., 1995. Late Holocene advance of the müller ice shelf, antarctic Peninsula: sedimentological, geochemical and palaeontological evidence. Antarct. Sci. 7, 159–170. https://doi.org/10.1017/S0954102095000228.

Domack, E.W., Jacobson, E.A., Shipp, S., Anderson, J.B., 1999. Late pleistocene-holocene retreat of the west antarctic ice-sheet system in the Ross sea: Part 2–Sedimentologic and stratigraphic signature. Geol. Soc. Am. Bull. 111, 1517–1536.

Domack, E.W., Leventer, A., Dunbar, R., Taylor, F., Brachfeld, S., Sjunneskog, C., Cowan, E., Daniels, J.W., Escutia, C., Evans, A., Eyles, N., Guyodo, Y., Ioio, M., Iwai, M., Kyte, F., Lauer, C., Maldonado, A., Morez, T., Osterman, L., Pudsey, C., Schuffert, J., Vigar, K., Weinheimer, A., Williams, T., Winter, D., Wolf-Welling, T.C.W., 2001. Chronology of the palmer deep site, antarctic Peninsula: a Holocene palaeoenvironmental reference for the circum-antarctic. Holocene 11, 1–9. https://doi.org/10.1191/095968301673881493.

Domack, E.W., Leventer, A., Root, S., Ring, J., Williams, E., Carlson, D., Hirshorn, E., Wright, W., Gilbert, R., Burr, G., 2003. Marine sedimentary record of natural environmental variability and recent warming in the Antarctic Peninsula. In: Domack, E., Leventer, A., Burnett, A., Bindschadler, R., Convey, P., Kirby, M. (Eds.), Antarctic Peninsula Climate Variability: Historial and Paleoenvironmental Perspectives. American Geophysical Union Antarctic Research Series, vol. 79, pp. 205–224.

Domack, E.W., Duran, D., Leventer, A., Ishman, S., Doane, S., McCallum, S., Amblas, D., Ring, J., Gilbert, R., Prentice, M., 2005. Stability of the larsen B ice shelf on the antarctic Peninsula during the Holocene epoch. Nature 436, 681–685. https://doi.org/10.1038/nature03908.

Ferrigno, J.G., Cook, A.J., Mathie, A.M., Williams, R.S.J., Swithinbank, C., Foley, K.M., Fox, A.J., Thomson, J.W., Sievers, J., 2008. Coastal-change and Glaciological Map of the Larsen Ice Shelf Area, Antarctica: 1940-2005. U. S. Geological Survey

Geologic Investigations Map Series Map I-2600-b, 1 map sheet, 28 p. text.
Francois, R., Altabet, M.A., Burckle, L.H., 1992. Glacial-interglacial changes in surface nitrate utilization in the Indian sector of the Southern Ocean as recorded by sediment $\delta^{15}N$. Paleoceanography 7, 589–606.
Fryxell, G.A., 1991. Comparison of winter and summer growth stages of the diatom *Eucampia Antarctica* from the Kerguelen Convergence Zone. In: Barron, J.A., Larsen, B. (Eds.), Proceedings of the Ocean Drilling Program, Scientific Results 119. College Station, TX (Ocean Drilling Program), pp. 675–685.
Fryxell, G.A., Prasad, A.K.S.K., 1990. *Eucampia Antarctica var. recta* (Mangin) stat. nov. (Biddulphiaceae, Bacillariophyceae): life stages at the Weddell Sea ice edge. Phycologia 29, 27–38.
Gersonde, R., Crosta, X., Abelmann, A., Armand, L., 2005. Sea-surface temperature and sea ice distribution of the Southern Ocean at the EPILOG Last Glacial Maximum–a circum-Antarctic view based on siliceous microfossil records. Quat. Sci. Rev. 24, 869–896.
Gordon, J.E., Harkness, D.D., 1992. Magnitude and geographic variation of the radiocarbon content in Antarctic marine life: implications for reservoir corrections in radiocarbon dating. Quat. Sci. Rev. 11, 697–708. https://doi.org/10.1016/0277-3791(92)90078-M.
Hall, B.L., Koffman, T., Denton, G.H., 2010. Reduced ice extent on the western Antarctic Peninsula at 700–970 cal. yr B.P. Geology 38, 635–638. https://doi.org/10.1130/G30932.1.
Hansom, J.D., Flint, C.P., 1989. Holocene ice fluctuations on brabant Island, antarctic Peninsula. Antarct. Sci. 1, 165–166. https://doi.org/10.1017/S0954102089000246.
Hillenbrand, C.-D., Larter, R.D., Dowdeswell, J.A., Ehrmann, W., Cofaigh, C.Ó., Benetti, S., Graham, A.G.C., Grobe, H., 2010. The sedimentary legacy of a palaeo-ice stream on the shelf of the southern Bellingshausen Sea: Clues to West Antarctic glacial history during the Late Quaternary. Quat. Sci. Rev. 29, 2741–2763. https://doi.org/10.1016/j.quascirev.2010.06.028.
Hodgson, D.A., Roberts, S.J., Smith, J.A., Verleyen, E., Sterken, M., Labarque, M., Sabbe, K., Vyverman, W., Allen, C.S., Leng, M.J., Bryant, C., 2013. Late Quaternary environmental changes in Marguerite Bay, Antarctic Peninsula, inferred from lake sediments and raised beaches. Quat. Sci. Rev. 68, 216–236. https://doi.org/10.1016/j.quascirev.2013.02.002.
Hofmann, E.E., Klinck, J.M., Lascara, C.M., Smith, D.A., 1996. Water mass distribution and circulation west of the Antarctic Peninsula and including Bransfield Strait. In: Ross, R.M. (Ed.), Foundations for Ecological Research West of the Antarctic Peninsula 70. American Geophysical Union, Washington DC, pp. 61–80.
Horn, M.G., Robinson, R.S., Rynearson, T.A., Sigman, D.M., 2011. Nitrogen isotopic relationship between diatom-bound and bulk organic matter of cultured polar diatoms. Paleoceanography 26, PA3208,. https://doi.org/10.1029/2010PA002080.
Ingólfsson, Ó., Hjort, C., Berkman, P.A., Björck, S.E.C., Goodwin, I.D., Hall, B., Hirakawa, K., Melles, M., Möller, P., Prentice, M.L., 1998. Antarctic glacial history since the Last Glacial Maximum: an overview of the record on land. Antarct. Sci. 61, 326–344.
Ishman, S.E., Domack, E.W., 1994. Oceanographic controls on benthic foraminifers from the Bellingshausen margin of the Antarctic Peninsula. Mar. Micropaleontol. 24, 119–155.
Jacobs, S.S., Fairbanks, R.G., Horibe, Y., 1985. Origin and evolution of water masses near the Antarctic continental margin: evidence from $H_2^{18}O/H_2^{16}O$ ratios in seawater. In: Jacobs, S.S. (Ed.), Oceanology of the Antarctic Continental Shelf. American Geophysical Union, Washington DC, pp. 59–85. https://doi.org/10.1029/AR043p0059.
Jenkins, A., Jacobs, S., 2008. Circulation and melting beneath George VI ice shelf, Antarctica. J. Geophys. Res. 13 https://doi.org/10.1029/2007JC004449. C04013.
King, J.C., 1994. Recent climate variability in the vicinity of the Antarctic Peninsula. Int. J. Climatol. 14, 357–369.
Klinck, J.M., 1998. Heat and salt changes on the continental shelf west of the Antarctic Peninsula between January 1993 and January 1994. J. Geophys. Res. 103, 7617–7636.
Klinck, J.M., Hofmann, E.E., Beardsley, R.C., Salihoglu, B., Howard, S., 2004. Water-mass properties and circulation on the west Antarctic Peninsula continental shelf in austral fall and winter 2001. Deep-Sea Res. II 51, 1925–1946.
Larter, D.R., Anderson, J.B., Graham, A.G.C., Gohl, K., Hillenbrand, C.-D., Jakobsson, M., Johnson, J.S., Kuhn, G., Nitsche, F.O., Smith, J.A., Witus, A.E., Bentley, M.J., Dowdeswell, J.A., Ehrmann, W., Klages, J.P., Lindow, J., Cofaigh, C.Ó., Spiegel, C., 2014. Reconstruction of changes in the Amundsen Sea and Bellingshausen Sea sector of the west antarctic ice sheet since the last glacial maximum. Quat. Sci. Rev. 100, 55–86. https://doi.org/10.1016/j.quascirev.2013.10.016.
Lee, S.H., Kim, B.K., Joo, H.-T., Park, J.W., Lee, J.H., Joo, H.-M., Lee, D.B., Kang, C.-K., Kang, S.-H., 2015. Carbon contribution of sea ice floes in the Arctic Ocean. Deep-Sea Res. II. Topical Studies in Oceanography 120, 35–42.
Leventer, A., Domack, E.W., Ishman, S.E., Brachfeld, S., McClennen, C.E., Manley, P., 1996. Productivity cycles of 200–300 years in the Antarctic Peninsula region: understanding linkages among the sun, atmosphere, oceans, sea ice, and biota. Geol. Soc. Am. Bull. 108, 1626–1644. https://doi.org/10.1130/0016-7606(1996)108<1626:PCOYIT>2.3.CO;2.
Leventer, A., Domack, E., Barkoukis, A., McAndrews, B., Murray, J., 2002. Laminations from the palmer deep: a diatom-based interpretation. Paleoceanography 17, 3–15. PAL 3-1–PAL.
Martinson, D.G., Stammerjohn, S.E., Iannuzzi, R.A., Smith, R.C., Vernet, M., 2008. Western Antarctic Peninsula physical oceanography and spatio-temporal variability. Deep-Sea Res. II 55, 1964–1987.
Meredith, M.P., Wallace, M.I., Stammerjohn, S.E., Renfrew, I.A., Clarke, A., Venables, H.J., Shoosmith, D.R., Souster, T., Leng, M.J., 2010. Changes in the freshwater composition of the upper ocean west of the Antarctic Peninsula during the first decade of the 21st centry. Prog. Oceanogr. 87, 127–143.
Milliken, K.T., Anderson, J.B., Wellner, J.S., Bohaty, S.M., Manley, P.L., 2009. High-resolution Holocene climate record from Maxwell Bay, south Shetland islands, Antarctica. Geol. Soc. Am. Bull. 121, 1711–1725. https://doi.org/10.1130/B26478.1.
Mitchell, B.G., Holm-Hansen, O., 1991. Observations and modeling of the Antarctic phytoplankton crop in relation to mixing depth. Deep-Sea Res. 38, 981–1007.
Moffat, C., Owns, B., Beardsley, R.C., 2009. On the characteristics of circumpolar deep water intrusions to the west Antarctic Peninsula continental shelf. J. Geophys. Res. 114, 16,. https://doi.org/10.1029/2008JC004955.
Montes-Hugo, M., Doney, S.C., Ducklow, H.W., Fraser, W., Martinson, D., Stammerjohn, S.E., Schofield, O., 2009. Recent changes in phytoplankton communities associated with rapid regional climate change along the western Antarctic Peninsula. Science 323, 1470–1473.
Mortlock, R.A., Froelich, P.N., 1989. A simple method for the rapid determination of opal in pelagic marine sediments. Deep-Sea Res. 36, 1415–1426.
Mulvaney, R., Abram, N.J., Hindmarsh, R.C.A., Arrowsmith, C., Fleet, L., Triest, J., Sime, L.C., Alemany, O., Foord, S., 2012. Recent Antarctic Peninsula warming relative to Holocene climate and ice-shelf history. Nature 489, 141–144. https://doi.org/10.1038/nature11391.
Panizzo, V., Crespin, J., Crosta, X., Shemesh, A., Massé, G., Yam, R., Mattielli, N., Cardinal, D., 2014. Sea ice diatom contributions to Holocene nutrient utilization in East Antarctica. Paleoceanography 29, 328–342. https://doi.org/10.1002/2014PA002609.
Peck, V.L., Allen, C.S., Kender, S., McClymont, E.L., Hodgson, D.A., 2015. Oceanographic variability on the West Antarctic Peninsula during the Holocene and the influence of upper circumpolar deep water. Quat. Sci. Rev. 119, 54–65. https://doi.org/10.1016/j.quascirev.2015.04.002.
Reimer, P.J., Bard, E., Bayliss, A., Beck, J.W., Blackwell, P.G., Ramsey, C.B., Buck, C.E., Cheng, H., Edwards, R.L., Friedrich, M., Grootes, P.M., Guilderson, T.P., Haflidason, H., Hajdas, I., Hatté, C., Heaton, T.J., Hoffmann, D.L., Hogg, A.G., Hughen, K.A., Kaiser, K.F., Kromer, B., Manning, S.W., Niu, M., Reimer, R.W., Richards, D.A., Scott, E.M., Southon, J.R., Staff, R.A., Turney, C.S.M., van der Plicht, J., 2013. IntCal13 and Marine13 Radiocarbon age calibration curves 0-50,000 years cal BP. Radiocarbon 55, 1869–1887.
Rignot, E., 2006. Changes in ice dynamics and mass balance of the Antarctic ice sheet. Philos. T. R. For. Soc. 364, 1637–1655.
Rignot, E., Mouginot, J., Morlighem, M., Seroussi, H., Scheuchi, B., 2014. Widespread, rapid grounding line retreat of pine Island, thwaites, Smith, and kohler glaciers, west Antarctica, from 1992 to 2011. Geophys. Res. Lett. 41, 3502–3509. https://doi.org/10.1002/2014GL060140.
Robinson, R.S., Sigman, D.M., 2008. Nitrogen isotopic evidence for a poleward decrease in surface nitrate within the ice age Antarctic. Quat. Sci. Rev. 27, 1076–1090.
Scherer, R.P., 1994. A new method for the determination of absolute abundance of diatoms and other silt-sized sedimentary particles. J. Paleolimnol. 12, 171–180.
Shevenell, A.E., Domack, E.W., Kernan, G.M., 1996. Record of Holocene palaeoclimate change along the antarctic Peninsula: evidence from glacial marine sediments, Lallemand fjord. Pap. Proc. R. Soc. Tasman. 130, 55–64.
Shevenell, A.E., Ingalls, A.E., Domack, E.W., Kelly, C., 2011. Holocene southern ocean surface temperature variability west of the antarctic Peninsula. Nature 470, 250–254. https://doi.org/10.1038/nature09751.
Sjunneskog, C., Taylor, F., 2002. Postglacial marine record of the palmer deep, antarctic Peninsula (ODP leg 178, site 1098): 1. Total diatom abundance. Paleoceanography 17. https://doi.org/10.1029/2000PA00563. PAL 4-1–PAL 4-8.
Sjunneskog, C., Winter, D., 2012. A diatom record of late Pliocene cooling from the Ross Sea continental shelf, AND-1B, Antarctica. Global Planet. Change 96–97, 87–96. https://doi.org/10.1016/j.gloplacha.2012.01.013.
Smith, D.A., Klinck, J.M., 2002. Water properties on the west Antarctic Peninsula continental shelf: a model study of effects of surface fluxes and sea-ice. Deep-Sea Res. II 49, 4863–4886.
Smith, R.C., Stammerjohn, S.E., 2001. Variations of surface air temperature and sea ice extent in the western Antarctic Peninsula (WAP) region. Ann. Glaciol. 33, 493–500.
Smith, D.A., Hofmann, E.E., Klinck, J.M., Lascara, C.M., 1999. Hydrography and circulation of the west Antarctic Peninsula continental shelf. Deep-Sea Res. 46, 925–949.
Smith, J.A., Bentley, M.J., Hodgson, D.A., Roberts, S.J., Leng, M.J., Lloyd, J.M., Barrett, M.S., Bryant, C., Sugden, D.E., 2007a. Oceanic and atmospheric forcing of early Holocene ice shelf retreat, George VI Ice Shelf, Antarctica Peninsula. Quat. Sci. Rev. 26, 500–516.
Smith Jr., K.L., Robison, B.H., Helly, J.J., Kaufmann, R.S., Ruhl, H.A., Shaw, T.J., Twining, B.S., Vernet, M., 2007b. Free-drifting icebergs: hotspots of chemical and biological enrichment in the Weddell Sea. Science 317, 478–482. https://doi.org/10.1126/science.1142834.
Stammerjohn, S.E., Martinson, D.G., Smith, R.C., Ianuzzi, R.A., 2008. Sea ice in the western Antarctic Peninsula region: spatio-temporal variability from ecological and climate change perspectives. Deep-Sea Res. II 55, 2041–2058.
Strelin, J., Sone, T., Mori, J., Torielli, C., Nakamura, T., 2006. New data related to Holocene landform development and climatic change from James Ross Island, antarctic Peninsula. In: Fütterer, D., Damaske, D., Kleinschmidt, G., Miller, H., Tessensohn, F. (Eds.), Antarctica: Contributions to Global Earth Sciences.

Springer-Verlag, pp. 455–460.
Studer, A.S., Sigman, D.M., Martínez-García, A., Benz, V., Winckler, G., Kuhn, G., Esper, O., Lamy, F., Jaccard, S.L., Wacker, L., Oleynik, S., Gersonde, R., Haug, G.H., 2015. Antarctic Zone nutrient conditions during the last two glacial cycles. Paleocenaography 30, 845–862. https://doi.org/10.1002/2014PA002745.
Stuiver, M., Reimer, P.J., 1993. Extended 14C database and revised CALIB radiocarbon calibration program. Radiocarbon 35, 215–230.
Taylor, F., Whitehead, J., Domack, E., 2001. Holocene paleoclimate change in the Antarctic Peninsula: evidence from the diatom sedimentary and geochemical record. Mar. Micropaleontol. 41, 25–43.
The RAISED Consortium, Bentley, M.J., Cofaigh, C.Ó., Anderson, J.B., Conway, H., Davies, B., Graham, A.G.C., Hillenbrand, C.-D., Hodgson, D.A., Jamieson, S.S.R., Larter, R.D., Mackintosh, A., Smith, J.A., Verleyen, E., Ackert, R.P., Bart, P.J., Berg, S., Brunstein, D., Canals, M., Colhoun, E.A., Crosta, X., Dickens, W.A., Domack, E., Dowdeswell, J.A., Dunbar, R., Ehrmann, W., Evans, J., Favier, V., Fink, D., Fogwill, C.J., Glasser, N.F., Gohl, K., Golledge, N.R., Goodwin, I., Gore, D.B., Greenwood, S.L., Hall, B.L., Hall, K., Hedding, D.W., Hein, A.S., Hocking, E.P., Jakobsson, M., Johnson, J.S., Jomelli, V., Jones, R.S., Klages, J.P., Kristoffersen, Y., Kuhn, G., Leventer, A., Licht, K., Lilly, K., Lindow, J., Livingstone, S.J., Massé, G., McGlone, M.S., McKay, R.M., Melles, M., Miura, H., Mulvaney, R., Nel, W., Nitsche, F.O., O'Brien, P.E., Post, A.L., Roberts, S.J., Saunders, K.M., Selkirk, P.M., Simms, A.R., Spiegel, C., Stolldorf, T.D., Sugden, D.E., van der Putten, N., van Ommen, T., Verfaillie, D., Vyverman, W., Wagner, B., White, D.A., Witus, A.E., Zwartz, D., 2014. A community-based geological reconstruction of antarctic ice sheet deglaciation since the last glacial maximum. Quat. Sci. Rev. 100, 1–9. https://doi.org/10.1016/j.quascirev.2014.06.025.
Turner, J., Colwell, S.R., Marshall, G.J., Lachlan-Cope, T.A., Carelton, A.M., Jones, P.D., Lagun, V., Reid, P.A., Iagovkina, S., 2005. Antarctic climate change during the last 50 years. Int. J. Climatol. 25, 279–294.
Vaughan, D.G., Marshall, G.J., Connolley, W.M., Parkinson, C., Mulvaney, R., Hodgson, D.A., King, J.C., Pudsey, C.J., Turner, J., 2003. Recent rapid regional climate warming on the Antarctic Peninsula. Climatic Change 60, 243–274.